Transition probabilities in neutron-rich ^{84,86}Se

J. Litzinger,[1,*] A. Blazhev,[1] A. Dewald,[1] F. Didierjean,[2,3] G. Duchêne,[2,3] C. Fransen,[1] R. Lozeva,[2,3] K. Sieja,[2,3] D. Verney,[4] G. de Angelis,[5] D. Bazzacco,[6] B. Birkenbach,[1] S. Bottoni,[7] A. Bracco,[7] T. Braunroth,[1] B. Cederwall,[8] L. Corradi,[5] F. C. L. Crespi,[7] P. Désesquelles,[9] J. Eberth,[1] E. Ellinger,[1] E. Farnea,[6] E. Fioretto,[5] R. Gernhäuser,[10] A. Goasduff,[2,3,9] A. Görgen,[11,12] A. Gottardo,[4] J. Grebosz,[13] M. Hackstein,[1] H. Hess,[1] F. Ibrahim,[4] J. Jolie,[1] A. Jungclaus,[14] K. Kolos,[4] W. Korten,[11] S. Leoni,[7] S. Lunardi,[6] A. Maj,[13] R. Menegazzo,[15] D. Mengoni,[6,16] C. Michelagnoli,[6,17] T. Mijatovic,[18] B. Million,[19] O. Möller,[20] V. Modamio,[5] G. Montagnoli,[6] D. Montanari,[6] A. I. Morales,[7] D. R. Napoli,[5] M. Niikura,[4] G. Pollarolo,[21] A. Pullia,[7] B. Quintana,[22] F. Recchia,[6] P. Reiter,[1] D. Rosso,[5] E. Sahin,[5] M. D. Salsac,[11] F. Scarlassara,[6] P.-A. Söderström,[23] A. M. Stefanini,[5] O. Stezowski,[24] S. Szilner,[18] Ch. Theisen,[11] J. J. Valiente Dobón,[5] V. Vandone,[7] and A. Vogt[1]

[1]*Institut für Kernphysik, Universität zu Köln, D-50937 Köln, Germany*
[2]*Université de Strasbourg, IPHC, F-67037 Strasbourg, France*
[3]*CNRS, F-67037 Strasbourg, France*
[4]*Institut de Physique Nucléaire, CNRS/IN2P3 and Université Paris Sud, F-91405 Orsay, France*
[5]*Istituto Nazionale di Fisica Nucleare, Laboratori Nazionali di Legnaro, I-35020 Legnaro, Italy*
[6]*Istituto Nazionale di Fisica Nucleare, Sezione di Padova, and Università di Padova, I-35131 Padova, Italy*
[7]*Dipartimento di Fisica, Università di Milano, and INFN, Sezione di Milano, I-20133 Milano, Italy*
[8]*Department of Physics, Royal Institute of Technology, SE-10691 Stockholm, Sweden*
[9]*Centre de Spectrométrie Nucléaire et de Spectrométrie de Masse CSNSM, CNRS/IN2P3, and Université Paris-Sud, F-91405 Orsay Campus, France*
[10]*Physics Department E12, Technische Universität München, D-85748 Garching, Germany*
[11]*Institut de Recherche sur les lois Fondamentales de l'Univers- IRFU, CEA/DSM, Centre CEA de Saclay, F-91191 Gif-sur-Yvette Cedex, France*
[12]*Department of Physics, University of Oslo, P.O. Box 1048 Blindern, N-0316 Oslo, Norway*
[13]*The Henry Niewodniczański Institute of Nuclear Physics, Polish Academy of Sciences, ul. Radzikowskiego 152, 31-342 Kraków, Poland*
[14]*Instituto de Estructura de la Materia, CSIC, Madrid, E-28006 Madrid, Spain*
[15]*Istituto Nazionale di Fisica Nucleare, Sezione di Padova, I-35131 Padova, Italy*
[16]*Nuclear Physics Research Group, University of the West of Scotland, High Street, Paisley, Pa1 2Be, Scotland, United Kingdom*
[17]*GANIL, CEA/DSM-CNRS/IN2P3,BP 55027, F-14076 Caen Cedex 5, France*
[18]*Ruder Bošković Institute, HR-10002 Zagreb, Croatia*
[19]*Istituto Nazionale di Fisica Nucleare, Sezione di Milano, I-20133 Milano, Italy*
[20]*Institut für Kernphysik, Technische Universität Darmstadt, D-64289 Darmstadt, Germany*
[21]*Dipartimento di Fisica Teorica dell' Università di Torino and INFN, I-10125 Torino, Italy*
[22]*Laboratorio de Radiaciones Ionizantes, Universidad de Salamanca, E-37008 Salamanca, Spain*
[23]*Department of Physics and Astronomy, Uppsala University, SE-75120 Uppsala, Sweden*
[24]*Université de Lyon, Université Lyon-1, IN2P3/CNRS, F-69622 Villeurbanne Cedex, France*

(Received 23 November 2015; published 29 December 2015)

Reduced quadrupole transition probabilities for low-lying transitions in neutron-rich ^{84,86}Se are investigated with a recoil distance Doppler shift (RDDS) experiment. The experiment was performed at the Istituto Nazionale di Fisica Nucleare (INFN) Laboratori Nazionali di Legnaro using the Cologne Plunger device for the RDDS technique and the AGATA Demonstrator array for the γ-ray detection coupled to the PRISMA magnetic spectrometer for an event-by-event particle identification. In ^{86}Se the level lifetime of the yrast 2_1^+ state and an upper limit for the lifetime of the 4_1^+ state are determined for the first time. The results of ^{86}Se are in agreement with previously reported predictions of large-scale shell-model calculations using Ni78-I and Ni78-II effective interactions. In addition, intrinsic shape parameters of lowest yrast states in ^{86}Se are calculated. In semimagic ^{84}Se level lifetimes of the yrast 4_1^+ and 6_1^+ states are determined for the first time. Large-scale shell-model calculations using effective interactions Ni78-II, JUN45, jj4b, and jj4pna are performed. The calculations describe $B(E2; 2_1^+ \rightarrow 0_1^+)$ and $B(E2; 6_1^+ \rightarrow 4_1^+)$ fairly well and point out problems in reproducing the experimental $B(E2; 4_1^+ \rightarrow 2_1^+)$.

DOI: 10.1103/PhysRevC.92.064322 PACS number(s): 23.20.−g, 21.10.Tg, 21.60.Cs, 27.50.+e

I. INTRODUCTION

The nuclear structure of neutron-rich Se nuclei was the subject of many experimental and theoretical works in the last decade. The evolution of collectivity from stable selenium

*jlitzinger@ikp.uni-koeln.de

mid-shell isotopes up to the $N = 50$ shell closure was investigated experimentally and theoretically with great effort [1–6]. Recently this work was extended to nuclei with $N > 50$ [7–9]. So far mainly low and medium spin excitations of the yrast bands of ^{84,86}Se have been observed [2,4,5,9,10].

Investigation of low and medium spin levels in ^{86}Se is of particular interest and the assignment of the yrast 6_1^+ state was disputed in previous years. The recent study of ^{86}Se and ^{88}Kr with γ-ray spectroscopy methods [9,10] led to a revised level scheme of ^{86}Se. The yrast 6_1^+ state was replaced by a new candidate with $E = 2846$ keV suggesting a large energy gap between the yrast 6_1^+ and 4_1^+ levels (E_{6^+}-$E_{4^+} \approx 1300$ keV) [9].

This can be explained by the configuration of the 6_1^+ state, which can either be formed by coupling a 4_1^+ neutron configuration to a 2_1^+ proton configuration, causing a rise in excitation energy compared to the 4_1^+ state because of the breakup of a proton pair. Alternatively, the 6_1^+ state can be formed with a purely neutron configuration by exciting a neutron from the $d_{5/2}$ to the $g_{7/2}$ orbital, which also requires more energy from the energy gap between the $d_{5/2}$ and $g_{7/2}$ orbitals in this region of the nuclear chart. Such an energy gap between the yrast 6_1^+ and the yrast 4_1^+ level was observed in neighboring $N = 52$ isotones as well [9].

Large-scale shell-model calculations of nuclei with $Z = 30$–36 and $N = 52$–54 (including ^{86}Se) were recently performed [8–10]. These calculations reproduce excitation energies of the known low-lying yrast states in ^{86}Se within 150 keV. Up to now no comparison of $B(E2)$ values with experimental data was possible. In Ref. [8] a deformation analysis based on these shell-model calculations was carried out. In those cases where evidence of deformation and triaxiality show up, symmetry conserved configuration mixing (SCCM)-Gogny calculations were performed as well. According to these calculations, the ground-state bands of $N = 54$ isotones in zinc, germanium, and krypton lack the characteristic features of deformation, whereas in selenium deformation of the yrast band is predicted [8]. Experimental $B(E2)$ strengths from lifetime measurements would enable testing these predictions and investigating the nuclear shape parameters.

The nucleus ^{84}Se also shows interesting structures at medium spin excitations. Similar to the even-even neighbor isotone ^{86}Kr a cascade $7^+ \rightarrow 6^+ \rightarrow 5^+$ with excitation energies close to the ones in ^{84}Se is observed (compare Figs. 2 and 3 in Ref. [4]) which in the case of ^{86}Kr is part of the yrast cascade. These 7^+, 6^+, 5^+ states are interpreted as being part of the neutron particle-hole $\nu g_{9/2}^{-1} d_{5/2}^1$ multiplet [4,11].

Further on, in ^{84}Se the proposed yrast 6_1^+ level has an excitation energy of 3370 keV, close below the first 5_1^+ state, and decays solely to the yrast 4_1^+ state [4,5]. Such a level arrangement was not observed in other $N = 50$ nuclei in this region of the nuclear chart. Unlike the aforementioned 6_2^+ state of neutron character, this tentative 6_1^+ state, similarly to the yrast 2_1^+ and 4_1^+ states, should be of proton character. So far no definite experimental spin and parity determination of this 6_1^+ level in ^{84}Se was possible and the current assignment is based on comparison to shell-model calculations [4,5]. Thus $B(E2)$ values from lifetime measurements of these low- and medium-spin states would give further experimental benchmark to test the spin and parity assignments.

Experimental data on transition probabilities in this mass region are very sparse. For $N = 50$ isotones including ^{84}Se $B(E2\uparrow; 2_1^+ \rightarrow 0_1^+)$ values were measured via Coulomb excitation [1]. In addition to this, there are no further experimental data on reduced transition strengths in ^{84,86}Se. This motivates lifetime measurements in these neutron-rich Se isotopes.

II. EXPERIMENTAL DETAILS

Using the Cologne Plunger device for deep-inelastic reactions [12] an RDDS experiment was performed at the INFN, Legnaro, Italy. ^{86}Se (^{84}Se) nuclei were produced via a $+4n$ ($+2n$) transfer reaction induced by a ^{82}Se beam provided by the Tandem-XTU and the ALPI superconducting LINAC accelerator at an energy of 577 MeV. The beam impinged on a ^{238}U plunger target with a thickness of 2 mg/cm which was evaporated onto a 1.2-mg/cm Ta backing facing the beam. The target was produced at GSI Helmholtz Centre for Heavy Ion Research in Darmstadt. In the plunger device a ^{93}Nb degrader foil with a thickness of 4.1 mg/cm was mounted downstream. The degrader foil is used to slow down the projectilelike recoils before entering the PRISMA magnetic spectrometer [13–16]. The degrader thickness was chosen optimized to provide sufficient energy loss needed for a clean target and degrader peak separation and to leave sufficient recoil energy to ensure a good mass resolution with PRISMA. During five days effective beam time, three different target-to-degrader distances were measured. γ rays of the deexciting reaction products were detected with the AGATA spectrometer in its demonstrator configuration [17,18] which consisted of five triple clusters [19], each built up of three High Purity Germanium (HPGe) crystals. Each of these crystals is 36-fold segmented, which allows for an accurate reconstruction of each γ-ray interaction point with the detector material using an online pulse-shape analysis. This information was used by the tracking algorithm which reconstructed the trajectories of the incident photons to determine their energy, direction [18], and the angle of the γ rays with respect to the velocity vector of the scattered ion from the first interaction point.

Information from the detectors of the PRISMA spectrometer array were combined for the event-by-event identification of the projectilelike reaction products. PRISMA was set to $\theta_{\text{lab}} = 58^\circ$ with respect to the beam axis. The identification of atomic number Z was obtained using the $\Delta E/E$ method; see Fig. 1. Energy loss and total energy of the ions were measured in a 10×4 fold (width $\times$ depth, respectively) segmented ionization chamber positioned at the end of the focal plane of PRISMA. Although the Z resolution in the $\Delta E_{\text{IC}} - E_{\text{IC}}$ matrix was not ideal we see no transitions from neighboring Z nuclei in the $Z = 34$ gated γ-ray spectra.

The mass determination was performed via the t_{TOF}-Bρ technique. The position information of the recoils was measured at the entrance microchannel plate (MCP) detector and at the focal plane multiwire parallel-plate avalanche counters (MWPPAC). In addition, these detectors were used as a stop

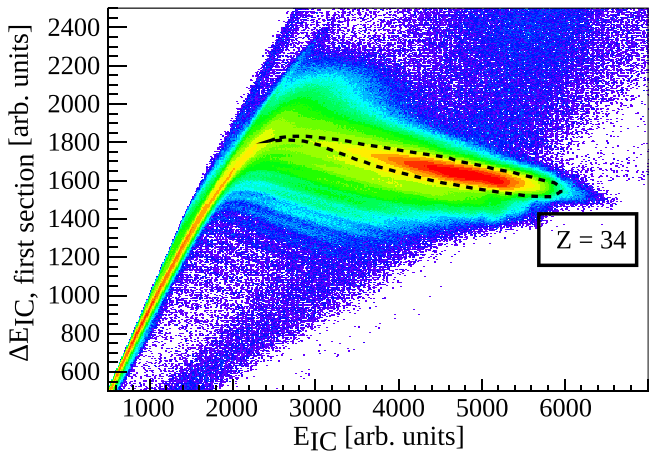

FIG. 1. (Color online) $\Delta E_{\mathrm{IC}}/E_{\mathrm{IC}}$ matrix for the identification of the atomic number Z.

and start signal for a time-of-flight t_{TOF} measurement. A trajectory reconstruction algorithm uses the position and time signals given by the entrance MCP detector and the focal-plane MWPPAC detector and the strength of the magnetic fields for an iterative, event-by-event reconstruction of the trajectory length L and the curvature radius ρ inside the Dipole magnet. From L and t_{TOF} the velocity vector of the recoils is reconstructed.

The ratio A/q is obtained using the relation,

$$\frac{A}{q} = \frac{B\rho t_{\mathrm{TOF}}}{L},$$

where B denotes the magnetic field and L is the trajectory length.

Different atomic charge states are separated using the relation,

$$q = \frac{2E_{\mathrm{IC}}t_{\mathrm{TOF}}}{B\rho L} \propto \frac{E_{\mathrm{IC}}}{\rho\beta},$$

by setting two-dimensional gates in the corresponding $E_{\mathrm{IC}} - \rho\beta$ matrix. In the above relation E_{IC} is the kinetic energy of the ion measured in the ionization chamber and $\beta = v/c$ is the recoil velocity.

An average mass resolution of $\frac{m}{\Delta m} \approx 235$ was achieved (see Fig. 2), which is sufficient to separate the Se isotopes.

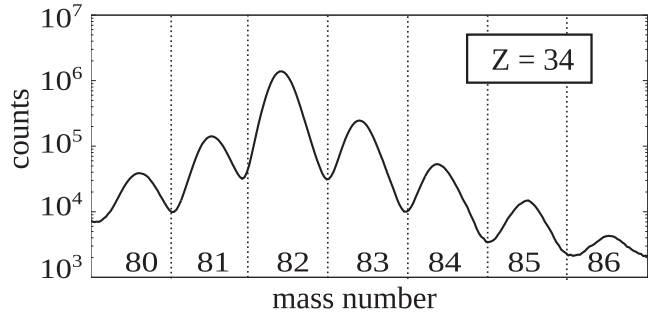

FIG. 2. Mass distribution for $Z = 34$. An average mass resolution of $\frac{m}{\Delta m} \approx 235$ was achieved.

Normalized experimental cross sections of the $+2n(+4n)$ neutron transfer channels ^{84}Se(^{86}Se) are 0.3(0.014). These numbers are given relative to the $+1n$ reaction channel ^{83}Se. By comparing these normalized experimental cross sections to calculations using the program code GRAZING [20] we find that experimentally determined relative cross sections drop faster than calculated ones. This results in very limited statistics for ^{86}Se.

The Doppler correction of the γ rays was performed using the angular information deduced from the first γ-ray interaction point provided by the AGATA detectors and the velocity vector provided by PRISMA. Therefore, the particle velocity after passing the degrader foil is used for the Doppler correction. After the Doppler correction the degraded component occurs at the nominal γ energy whereas the fast component is shifted to lower energies, as AGATA was located at backwards angles.

Assuming a binary reaction and imposing the conservation of linear momentum, the total kinetic energy loss (TKEL) of the recoils is reconstructed event-by-event using relativistic two-body reaction kinematics [15,21]. ^{84}Se gated γ-ray spectra are generated with a condition on TKEL to clean them up.

III. LIFETIME ANALYSIS

The lifetime of an excited state can be determined from the decay curve, which is the intensity ratio of the degraded and the sum of fast and degraded peaks of γ rays depopulating the level of interest as a function of the distance d between the foils, $R(d) = I_D(d)/(I_D(d) + I_T(d))$ [22]. In case of a γ-singles analysis all observed feeding transitions (feeder) have to be taken into account. In this case the solution of the corresponding system of differential equations (Bateman equations), is fitted to the decay curve [12]. For such an analysis exact absolute distance information is crucial, especially when only few target-to-degrader distances were used.

The plunger device used provides nearly perfect relative distance information with a precision of $\approx$0.1 μm, but always with an offset caused by an unknown zero point which depends on the quality of the target and degrader surface. In this work absolute distance information was obtained by analyzing transitions with well-known level lifetimes in ^{82}Se [23], taking advantage of the high statistics in this reaction channel. ^{82}Se was excited via multiple-step Coulomb excitation and consequently, all feeders are known and unobserved side feeding can be excluded. With this method the three absolute target-to-degrader distances in this experiment were determined to 38(1) μm, 257(2) μm, and 507(7) μm. This corresponds to an offset of 19.6 μm.

A reduction of recoil velocity caused by the energy loss of the recoils in the degrader foil was calculated using the program LISE++ [24] with the ATIMA 1.2 algorithm ($\Delta\beta_{\mathrm{Deg.,LISE++}} = 1.64\%$) and compared to the experimentally observed Doppler shifts ($\Delta\beta_{\mathrm{Deg.,DS}} = 1.73\%$), which are in good agreement within 5% of the value. The velocity of the recoils after the target was calculated from the mean β values of the recoiling nuclei measured with PRISMA and the calculated energy loss in the degrader. A recoil velocity

of ≈9% for Se nuclei was determined, leading to particle flight times of ≈1.4, 10, and 19 ps for the three different target-to-degrader distances. Consequently, the experiment was sensitive to relative lifetimes from about 1 ps up to about 100 ps. For the lifetime analysis the recoil velocities were regarded individually as they depend on the gates that have been used.

After the particle identification process ^{86}Se γ-ray spectra showed up a significant contamination with γ rays from the ^{82}Se beam. In the $Z = 34$ $E_{IC} - \rho\beta$ matrix charge states with a gating condition on $A = 86$ showed substructures which were traced back to ^{82}Se nuclei by analyzing the coincident γ rays. This is a result of overlapping A/q values and could be drastically reduced by choosing smaller gates for charge states in case of ^{86}Se.

As we deal with velocities of $\beta \approx 9\%$ relativistic effects were taken into account which affect the peak intensities. The aberration effect, which causes a change of the solid angle because of the relativistic Lorentz transformation and the change of the emission angle in the laboratory system compared to the moving system (Lorentz boost) were taken into account.

Detector efficiencies were calculated using the GEANT4 TOOLKIT [25]. In addition, relative efficiencies of AGATA were measured using an ^{152}Eu source in an earlier experiment with identical experimental setup [26]. Efficiency spectra were collected using the same tracking algorithm that was used for in-beam data. Within the energy region of interest measured relative detector efficiencies are consistent with the calculated ones. For this analysis transition intensities were corrected with respect to detector efficiencies using the energy-dependent relation $\epsilon(E_\gamma) = E_\gamma^{-0.42}$, which corresponds to GEANT4 calculated values. In addition, different detector efficiencies of the shifted and unshifted component of one transition were considered.

A. ^{86}Se

Because of the very limited statistics in case of ^{86}Se, it was not possible to analyze the γ-ray spectra of each distance individually. Consequently, spectra for the three measured distances were added up. Figure 3 shows the resulting ^{86}Se γ spectrum centered on the energies of the $2_1^+ \rightarrow 0_1^+$ and $4_1^+ \rightarrow 2_1^+$ transition in ^{86}Se (704 keV and 863 keV, respectively). No other γ-ray transition of ^{86}Se is visible. Thus the $4_1^+ \rightarrow 2_1^+$ transition was considered as the sole feeder for the analysis of the 2_1^+ state. The $4_1^+ \rightarrow 2_1^+$ transition is visible with 81(9)% intensity of the $2_1^+ \rightarrow 0_1^+$ transition and considered as a feeder for the analysis of the 2_1^+ state; the remaining 19% feeding of this state is supposed to be fast compared to the decay of the 2_1^+ state. Here, and in the following, efficiency-corrected transition intensities are given. Because of summing up spectra of different target-to-degrader distances the lifetime is calculated from the solution of the differential Bateman equations as follows:

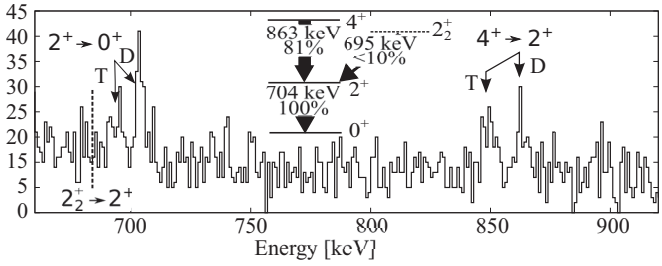

FIG. 3. γ spectrum of ^{86}Se. Because of limited statistics the spectra for all target-to-degrader distances were added up. The shifted component of a possible feeding transition with $E_\gamma = 694$ keV described in Ref. [10] is marked with a dashed line and discussed in the text. No stopped component is expected.

$$R_{\text{sum}} = \frac{\sum_{j=1}^{n} I_{Dj}}{\sum_{j=1}^{n} I_{Dj} + \sum_{j=1}^{n} I_{Tj}} = \sum_{j=1}^{n} n_j R(x_j), \qquad (1)$$

where I_{Dj} (I_{Tj}) denotes the degrader (target) component of each distance x_j, $R(x_j)$ is the decay curve, described by the solution of the Bateman equations, and n_j denotes normalization factors for each distance. For the actual case the lifetime of the 2_1^+ state is given from Eq. (1) by the solution of the expression,

$$R_{\text{sum}} - \sum_{j=1}^{3} n_j \left[0.19 e^{-\lambda_2 x_j} + \frac{0.81}{\frac{\lambda_2}{\lambda_4} - 1} \left(\frac{\lambda_2}{\lambda_4} e^{-\lambda_4 x_j} - e^{-\lambda_2 x_j} \right) \right] = 0. \qquad (2)$$

The decay constant of a level i, λ_i, is related to the level lifetime τ_i with $\tau_i = 1/\lambda_i$.

The experimentally observed intensity ratio of the $2_1^+ \rightarrow 0_1^+$ transition from the summed spectra [Eq. (1)] is $R_{\text{sum}} = 0.67(7)$ and marked in Fig. 4(a). The statistics of the different target-to-degrader distances were normalized using the number of nuclei in the PRISMA particle gate n_j for each distance j. The resulting $R(\tau)$ curve is shown in Fig. 4(a).

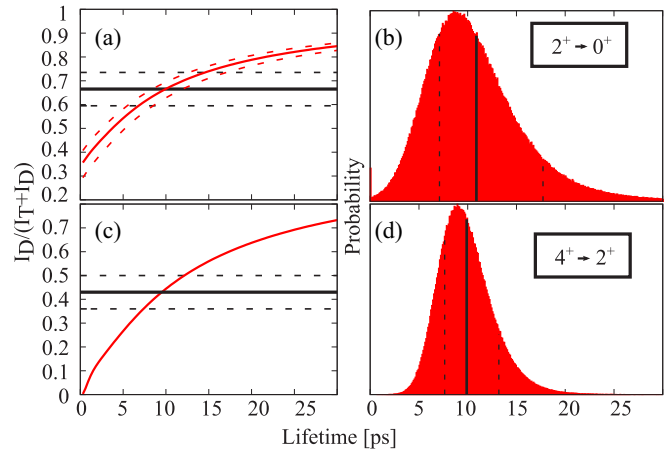

FIG. 4. (Color online) $R(\tau)$ curve (red) and error estimation for the $2_1^+ \rightarrow 0_1^+$ (a) and (b), and $4_1^+ \rightarrow 2_1^+$ (c) and (d) transition of ^{86}Se. Eighty percent feeding intensity of the $4_1^+ \rightarrow 2_1^+$ transition was included in the lifetime estimation of the 2_1^+ state. A lifetime of $\tau_{2^+} = 10.8(^{+69}_{-37-3})$ ps and a relative lifetime of $\tau_{4^+} = 9.9(^{+33}_{-22})$ ps was determined. No feeding transition of the 4_1^+ state was observed in the spectra, thus only an upper limit for the 4_1^+ lifetime can be given.

TABLE I. Summary of the experimental results for ^{86}Se compared to large-scale shell-model calculations from [8] using the Ni78-I effective interaction and from [10] using the Ni78-II interaction. Experimental γ-ray transition energies are taken from [9]. See text for further details.

A	$J^{\pi i} \rightarrow J^{\pi f}$	E_γ (keV)	Experiment			Theory	
			$\frac{\sum I_D}{(\sum I_D + \sum I_T)}$	$\tau(J^{\pi I})$ (ps)	$B(E2)$ (e^2 fm^4)	$B(E2)$ (e^{2}fm^4)	
						Ni78-I [8] $e_p = 1.7, e_n = 0.7$	Ni78-II [10] $e_p = 1.7, e_n = 0.7$
^{86}Se	$2_1^+ \rightarrow 0_1^+$	704.2(2)	0.67(7)	$10.8(^{+69}_{-37-3})$	$438(^{+259}_{-171})$	436	370
	$4_1^+ \rightarrow 2_1^+$	863.4(3)	0.44(7)	$9.9(^{+33}_{-22})$	> 140	439	395
	$6_1^+ \rightarrow 4_1^+$	1278.4(3)	–	–	-	607	505

Using this method, we extract a lifetime value for the 2_1^+ state of $\tau = 10.8(^{+69}_{-37-3})$ ps.

The error of the measured lifetimes was determined with a Monte Carlo simulation of the lifetime calculation with 10^6 iterations, taking into account the uncertainty of the intensity ratio [Eq. (1), left side] of the feeding transition and of the transition of interest, the uncertainty on absolute distance values and the uncertainty of the transition intensities. The expectation value of the generated distribution [solid line in Fig. 4(b)] corresponds to the value for the lifetime. Errors were deduced from the 1 σ quantiles of the probability distribution in both directions [dashed lines in Fig. 4(b)].

In an earlier experiment reported in Ref. [10] the decay out of the 2_2^+ state was observed stronger than the one from the 4_1^+ state. In this experiment ^{86}Se nuclei were produced via fission of actinides. In our case, however, because of the different reaction used, we see no hint of the 2_2^+ feeding transition; see Fig. 3. Taking into account the background in our experimental spectra, we have estimated that a feeding from such a 2_2^+ state to the 2_1^+ state would be below 10%. Therefore we investigated the influence of such a feeding on the 2_1^+ state lifetime for our reaction. For this simulation the lifetime of this 2_2^+ state is estimated conservatively from systematic considerations in this region with $\tau_{2_2^+} = 1.5$ ps; the intensity is assessed with 10%. A maximum reduction of the 2_1^+ lifetime of -0.3 ps was found and is included as systematical error; see Table I.

The intensity ratio for the $4_1^+ \rightarrow 2_1^+$ transition of the summed spectra is $R_{\rm sum} = 0.44(7)$; see Fig. 4(c). The resulting effective lifetime of the 4_1^+ state is $9.9(^{+33}_{-22})$ps; see Fig. 4(d). As we have no information on the feeding of the 4_1^+ state in this case only an upper lifetime limit of $\tau_{4^+} \leqslant 13.2$ ps can be given.

All values are summarized in Table I.

B. ^{84}Se

In Fig. 5 γ-ray spectra of ^{84}Se centered at the energy of the yrast $4_1^+ \rightarrow 2_1^+$ transition are shown, the evolution of the flight and degraded component with respect to the flight time between the target and the degrader foil is clearly visible. Three direct feeding transitions of the 4_1^+ state are observed, the $6_1^+ \rightarrow 4_1^+$, $5_1^+ \rightarrow 4_1^+$, and $6_2^+ \rightarrow 4_1^+$ transition with 13(3)%, 52(3)%, and 27(3)% intensity relative to the $4_1^+ \rightarrow 2_1^+$ transition, respectively.

As mentioned above, the level lifetime is determined from the decay curve taking all observed feeders with their effective lifetimes into account, fitted to the experimentally observed intensity ratios $I_D/(I_D+I_T)$. This leads to a level lifetime of $29.2(^{+59}_{-37})$ ps for the 4_1^+ state in ^{84}Se. The additional 8% unobserved feeding is assumed to be fast compared to the analyzed decay.

The yrast 6_1^+ state was populated with only 13% relative to the yrast 4_1^+ state, leading to limited statistics for a γ-ray spectra analysis distance-per-distance and resulting in large uncertainties for the target-to-degrader intensity ratios. As a consequence, the lifetime of the 6_1^+ state was analyzed as follows: (a) using the standard procedure similar to the 4_1^+ state (method 1) and (b) with the method described above and used for ^{86}Se (method 2). The latter is a useful cross-check for low statistic cases as the intensity ratio is much more robust against statistical background fluctuations.

In Fig. 6 γ-ray spectra of ^{84}Se centered at the energy of the yrast $4_1^+ \rightarrow 2_1^+$ transition are shown.

Two feeding transitions for the yrast 6_1^+ state were observed in former experiments. The first one with $E_\gamma = 492$ keV, also from a multineutron transfer experiment described in [2] could not be identified within this experiment. The other one with $E_\gamma = 1270$ keV was observed in a fission experiment described in Ref. [5].

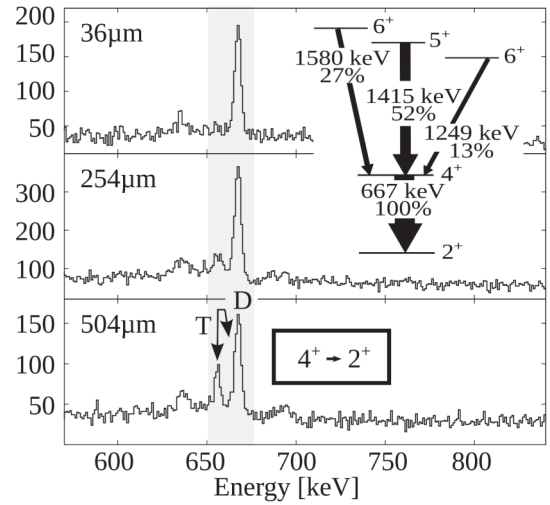

FIG. 5. γ-ray spectra of ^{84}Se centered at the energy of the yrast $4_1^+ \rightarrow 2_1^+$ transition, the three measured target-to-degrader distances are plotted on top of each other.

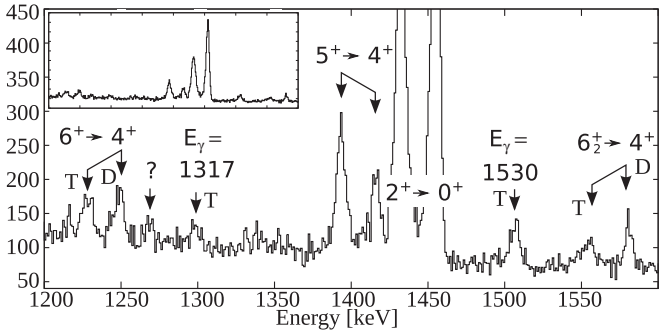

FIG. 6. γ spectrum of ^{84}Se from 1200 keV up to 1600 keV, showing the yrast $6_1^+ \rightarrow 4_1^+$, a possible feeding transition of the 6_1^+ state, and all feeding transitions of the 4_1^+ state. The three measured target-to-degrader distances are added up. For reason of clarity the dominating $2_1^+ \rightarrow 0_1^+$ transition was cut.

A very small peak with 15% intensity relative to the $6_1^+ \rightarrow 4_1^+$ transition at $E_\gamma = 1267$ keV is visible in the γ-ray spectra. This peak is caused by the feeding transition of the 6_1^+ state mentioned above, or by the flight component of a fast transition from a level at $E = 3408.7$ keV with $E_\gamma = 1287$ keV feeding the 4_1^+ state described in [27], or by a mixture of both. For this $E_\gamma = 1267$ keV transition in both cases no time behavior is visible, thus the lifetime of a possible 6_1^+ feeder would be long compared to the lifetime of the 6_1^+ state and therefore relevant for the lifetime analysis. The effect of level feeding was analyzed systematically for the 6_1^+ state lifetime. A simulation of the 6_1^+ state lifetime depending on the lifetime of a feeder with 15% intensity is shown in Fig. 7(a). The influence of the feeding intensity up to a maximum of 50% assuming the worst case with $\tau_{\text{Feeder}} = 150$ ps is shown in Fig. 7(b). The possibility of 15% level feeding with $\tau_{\text{Feeder}} = 150$ ps, leading to a maximum reduction of the 6_1^+ state lifetime of -3.4 ps, contributes systematically to the error of the 6_1^+ state lifetime.

For the sake of completeness, it should be mentioned that possible additional 4_1^+ state feeding from the $E_\gamma = 1287$ transition would not affect the 4_1^+ lifetime at all, as even for the shortest distance no time behavior is visible, thus its lifetime would be very fast compared to the decay of the 4_1^+ state.

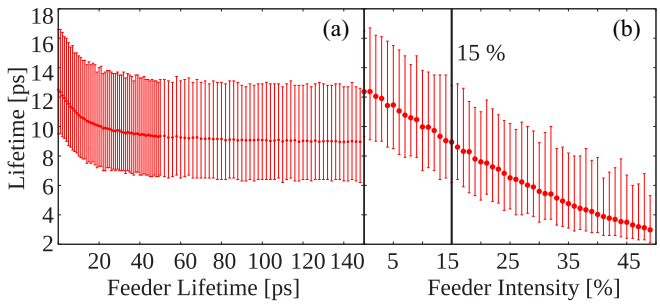

FIG. 7. (Color online) Simulation of level feeding effects. (a) Lifetime of the 6_1^+ state in ^{84}Se as a function of lifetime of a feeder with 15% intensity. (b) Influence of slow level feeding with $\tau_{\text{Feeder}} = 150$ ps on the resulting 6_1^+ state lifetime for ^{84}Se as a function of the feeder intensity.

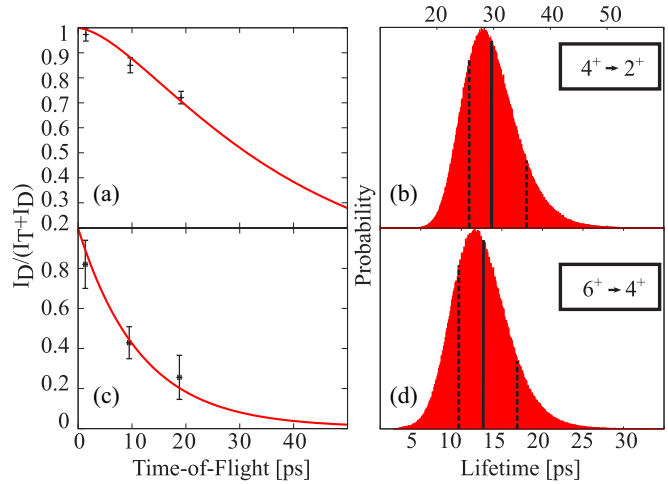

FIG. 8. (Color online) Decay curve, lifetime fit (red), and error distribution of the yrast $4_1^+ \rightarrow 2_1^+$ transition a) and (b), and $6_1^+ \rightarrow 4_1^+$ transition (c) and (d) in ^{84}Se. More details are given in the text.

Moreover, this transition has only <2% intensity compared to the level of interest.

In contrast to the feeding assumptions made for the 4_1^+ state in ^{86}Se, the yrast 6_1^+ state in ^{84}Se has a level energy of 3371 keV which is in the range of the highest level energies populated within the neutron transfer channels in this experiment. We suppose the feeding of this level to be dominated by fast statistical transitions from the continuum. Thus we assume the decay curve of the 6_1^+ state in ^{84}Se in this case to be mostly independent from feeding. It should be stressed here that the possibility of relevant side feeding cannot be completely ruled out and that in such a case the result given here has to be considered as an effective lifetime. But as we have good argument for the assumption made in this context we give the result of $\tau = 12.5(^{+44}_{-28-34})$ ps from method 1 and $\tau = 11.8(^{+25}_{-18-34})$ ps from method 2 for the yrast 6_1^+ state in ^{84}Se. The latter result is used for further theoretical discussions.

The decay curve for the yrast 4_1^+ and 6_1^+ state are shown in Figs. 8(a) and 8(c), respectively. The corresponding resulting lifetime distributions are depicted in Figs. 8(b) and 8(d).

The lifetime of the yrast 2_1^+ state in ^{84}Se was experimentally deduced from Coulomb excitation [1]. From the $B(E2\uparrow; 0_1^+ \rightarrow 2_1^+) = 0.105(15)\ e^2b^2$ [1] a level lifetime of $\tau_{2^+} = 0.60(9)$ ps was deduced. The present experiment is less sensitive to lifetimes < 1 ps, as the smallest target-to-degrader distance leads to recoil flight times of 1.34 ps between target and degrader for ^{84}Se. Furthermore, the time behavior of the $2_1^+ \rightarrow 0_1^+$ transition is dominated by the feeding of the yrast 4_1^+ state which has a much longer lifetime. Nevertheless, it is worth mentioning that by this analysis an upper lifetime limit of $\tau_{2_1^+} \leqslant 1$ ps can be estimated.

IV. DISCUSSION

The evolution of yrast 2_1^+, 4_1^+, and 6_1^+ excitation energies and the corresponding $2^+ \rightarrow 0^+$, $4^+ \rightarrow 2^+$, and $6^+ \rightarrow 4^+$ transition probabilities for the selenium and neighboring isotopic chains is shown in Fig. 9. For ^{84,86}Se the $B(E2)$

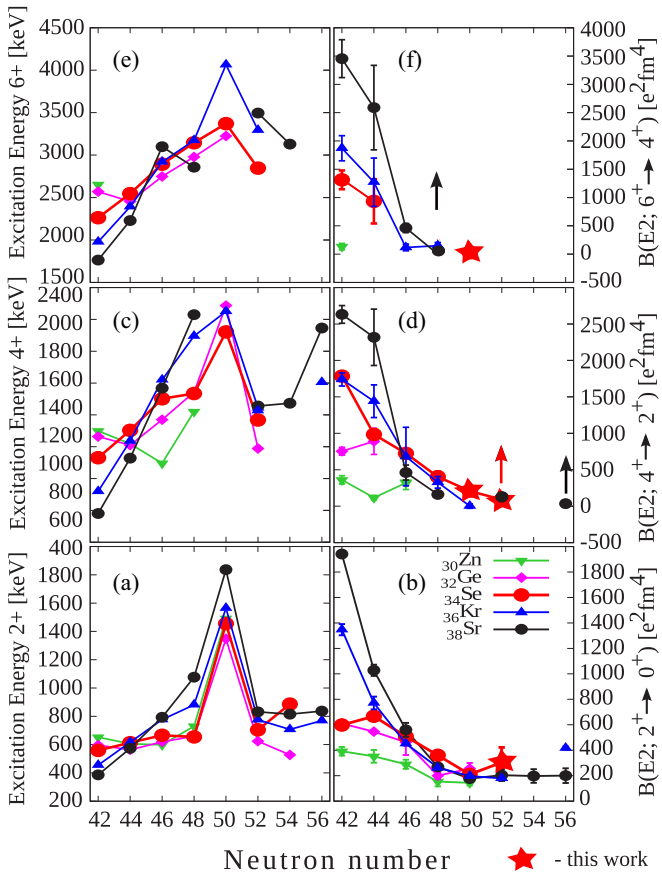

FIG. 9. (Color online) $2_1^+, 4_1^+$, and 6_1^+ excitation energies [(a), (c), and (e)] and corresponding $B(E2)$ systematics [(b), (d), and (f)] of Se and neighboring isotopic chains with $N = 42$–56. Values marked by a star are from this work; all other values are taken from NNDC.

systematics are complemented by our new values. Between $N = 42$ and $N = 48$ the 2_1^+ excitation energies of selenium isotopes remain somewhat constant at ≈600 keV and increase dramatically at $N = 50$ while corresponding $B(E2)$ values uniformly decrease. Nuclei with a closed neutron shell at $N = 50$ are characterized by a high 2_1^+ excitation energy and a small $2^+ \rightarrow 0^+$ transition probability. From $N = 50$ to $N = 52$ the 2_1^+ excitation energy decreases dramatically over all isotopes while the corresponding $B(E2; 2^+ \rightarrow 0^+)$ values stay nearly constant in case of Sr and Kr isotopes. For $N = 52$ ^{86}Se a small rise of the $B(E2; 2_1^+ \rightarrow 0^+)$ is indicated by our new value but with a large uncertainty.

The 4_1^+ (6_1^+) level energies in Se isotopes increase uniformly with the number of neutrons up to a maximum value of ≈ 2000 keV (≈3200 keV) at $N = 50$, while the corresponding $B(E2)$ values decrease much faster than those of the $2_1^+ \rightarrow 0^+$ transition. Our new experimental $B(E2; 4_1^+ \rightarrow 2_1^+)$ value for ^{84}Se fits into the Se systematics. The new $B(E2; 6_1^+ \rightarrow 4_1^+)$ value for ^{84}Se suggests a similar systematic behavior for the $6_1^+ \rightarrow 4_1^+$ as the $4_1^+ \rightarrow 2_1^+$ systematics [see Figs. 9(f) and 9(d)] but the B($E2$;$6_1^+ \rightarrow 4_1^+$) values for ^{80,82}Se are important to complete the Se systematics and would act as a benchmark for theoretical descriptions.

A. ^{86}Se

For $N = 52$ isotones with $32 \leqslant Z \leqslant 48$ the excitation energies of the yrast levels 2_1^+ and 4_1^+ seem to be nearly independent from Z; see Figs. 9(a) and 9(c). These excitations are expected to result from the coupling of the two valence neutrons in the $d_{5/2}$ orbital. As this configuration cannot create a 6_1^+ state the latter might be created by the coupling of a 4_1^+ neutron configuration to a 2_1^+ proton configuration or by exciting a neutron from the $d_{5/2}$ to the $g_{7/2}$ orbital. Both ways of forming a 6_1^+ state lead to a significant energy gap between the yrast 4_1^+ and 6_1^+ states as predicted by the shell-model calculations and confirmed by the latest experimental results; see Table I and Refs. [8,9]. These shell-model calculations for ^{86}Se were done with ^{78}Ni as an inert core, a $1f_{5/2}$, $2p_{3/2}$, $2p_{1/2}$, $1g_{9/2}$ valence space for protons and a $2d_{5/2}$, $3s_{1/2}$, $2d_{3/2}$, $1g_{7/2}$, $1h_{11/2}$ valence space for neutrons employing the shell-model codes ANTOINE [28] and NATHAN [29]. The effective interactions used in this $\pi r3g - \nu r4h$ model space, dubbed hereafter Ni78-I and Ni78-II, have been established and described in Ref. [30] and Refs. [10,31], respectively. In both cases, the electric transition strengths were calculated using $1.7e$ and $0.7e$ effective charges for protons and neutrons, respectively.

Referring to calculations with Ni78-I from [8,9], the wave functions of the 2_1^+ (4_1^+) state from shell-model diagonalizations come out as 44% (48%) of 0_1^+ proton configuration coupled to 2_1^+ (4_1^+) neutron configuration and 33% (31%) of 2_1^+ proton configuration coupled to 0_1^+ (2_1^+) neutron configuration. The 6_1^+ state is dominated with 81% by a 2_1^+ proton coupled to 4_1^+ neutron configuration. In terms of occupation probabilities, for neutrons the population of the $d_{5/2}$ orbital is 1.59, 1.56, 1.76, 1.87 for the 0_1^+, 2_1^+, 4_1^+, and 6_1^+ states, respectively. So based on the shell-model calculations these states seem indeed to be dominated by a $d_{5/2}^2$ configuration. On the proton side the occupations seem more spread between $f_{5/2}$, $p_{3/2}$ and even the $p_{1/2}$ and $g_{9/2}$ orbitals.

The configuration of $\pi f_{5/2}^4 p_{3/2}^2 \otimes \nu d_{5/2}^2$ is dominant with 47%, 39%, 49%, and 50% for the yrast 0_1^+, 2_1^+, 4_1^+, and 6_1^+ states, respectively. The occupation of the $g_{7/2}$ orbital for the yrast 6_1^+ state is only 0.1%. Thus the calculations do not seem to favor the neutron excitation from $d_{5/2}$ to $g_{7/2}$ to build the yrast 6_1^+ state.

The excitation energies of yrast levels in $N = 52$ isotones are described well within 150 keV by the calculations; the expected energy gap between the 4_1^+ and 6_1^+ state is also reproduced [9]. This supports the shell-model calculations which also give predictions for $B(E2)$ values for $N = 52$–54 isotones in the region of $Z = 30$–36 [8,9]. These theoretical $B(E2)$ values reproduce the experimental transition strengths of the present work fairly well within the uncertainties (see Table I). There is a fair agreement between our new experimentally deduced value of $B(E2; 2_1^+ \rightarrow 0^+) = 438(^{+259}_{-171})$ e^2 fm^4 and the theoretical $B(E2)$ value of 436 e^2 fm^4. For the yrast $4_1^+ \rightarrow 2_1^+$ transition the experimentally found lower limit of $B(E2; 4_1^+ \rightarrow 2_1^+) > 140$ e^2 fm^4 is compatible with the shell-model anticipation of 439 e^2 fm^4.

Extending the previous work [8] we investigated the nuclear deformation parameters of ^{86}Se yrast states, based on the

TABLE II. Intrinsic shape parameters of ^{86}Se based on shell-model calculations using Ni78-I.

J^π	Q_{intr} (e fm^2)	β	γ (deg.)
0^+_{gs}	162	0.22	22
2^+_1	159	0.22	21
4^+_1	151	0.21	22
6^+_1	136	0.19	12

shell-model calculations described above, using the n-body quadrupole operators introduced in Ref. [32].

The axial deformation parameter β is deduced from the intrinsic quadrupole moment Q_{intr} and the asymmetry angle γ is calculated. The results are summarized in Table II. Following these calculations ^{86}Se shows quite constant ground-state band deformation from 0^+_{gs} up to the first 6^+_1 state with $\beta \approx 0.2$. The asymmetry angle γ stays more or less constant for the 0^+, 2^+, 4^+ states with $\gamma = 21°$–$22°$ and falls to $\gamma = 12°$ for the 6+ state. This change of the nuclear shape towards the 6^+_1 state might be indicative for the aforementioned change in nuclear structure of the 6^+_1 state compared to the 0^+, 2^+, and 4^+ states. These calculations indicate triaxiality for the yrast 0^+_1, 2^+_1, and 4^+_1 states and might hint γ softness in medium spin states in ^{86}Se. Similar calculations for ^{88}Se (see Table 4 in Ref. [8]) also indicate a more or less constant, strong axial ground-state band deformation with $\beta \approx 0.25$ but with a lower asymmetry angle compared to ^{86}Se, $\gamma = 9°$, $12°$, $15°$, and $14°$ for the 0^+, 2^+, 4^+, and 6^+ states, respectively.

For ^{86}Se we add calculations with Ni78-II reported in [10]; see Table I. The excitation energies of yrast levels up to the 6^+_1 state in ^{86}Se are described within 190 keV. Predictions for $B(E2)$ values reproduce our experimental transition strengths of the $2^+_1 \rightarrow 0^+_1$ transition well within the uncertainties (see Table I). The experimentally found lower $B(E2)$ limit of the $4^+_1 \rightarrow 2^+_1$ transition does not contradict the shell-model calculated value. Calculations with Ni78-II are also performed for ^{84}Se; see Table III.

B. ^{84}Se

Lowest excited level arrangements of the $N = 50$ isotonic chain change with proton number. In ^{84}Se yrast 2^+_1 and 4^+_1 states and a tentative 6^+_1 state were observed. The 6^+_1 state has an excitation energy of $E = 3370$ keV and decays solely to the yrast 4^+_1 state with $E_\gamma = 1249$ keV [4,5], (see also Fig. 5). In ^{86}Kr low-lying yrast 2^+_1 and 4^+_1 states were observed but no low-lying 6^+_1 state was found. In ^{88}Sr only a low-lying yrast 2^+_1 state was experimentally observed. Those lowest yrast states in ^{84}Se, ^{86}Kr, and ^{88}Sr are assumed to have a proton structure [4]. In the extreme single-particle picture the ground-state of ^{84}Se has six protons in the $f_{5/2}$ orbital and an empty $p_{3/2}$ orbital. As the $\pi f_{5/2}$ and $\pi p_{3/2}$ orbitals are close in energy, low-lying excited levels can arise from the rearrangement and coupling of protons in this $f_{5/2}p_{3/2}$ subshell with a maximum spin of 6^+_1. The 6^+_1 state can be formed by a $\pi f^{-2}_{5/2} \otimes \pi p^2_{3/2}$ configuration or by a $\pi f^{-3}_{5/2} \otimes \pi p^3_{3/2}$ configuration.

The spin and parity assignment of the tentative 6^+_1 state in ^{84}Se is based on a comparison of the experimentally observed excitation energy to shell-model calculations involving the above-mentioned proton structure [4,5]. It is difficult to reach this nucleus experimentally with sufficient cross sections for an angular correlation measurement allowing for a spin and parity assignment of medium spin states, thus up to now an experimental validation of assumptions concerning the $E = 3370$ keV level is missing. In this respect, our new $B(E2)$ value of the tentative $6^+_1 \rightarrow 4^+_1$ transition is discussed further in the text by comparison to theory.

For comparison of the new experimental results for ^{84}Se we performed shell-model calculations using ^{56}Ni as an inert core with the $f_{5/2}pg_{9/2}$ valence orbitals and the JUN45 [33] and jj4b and jj4pna [34] effective interactions using the code NUSHELLX@MUS [35]. We used effective proton charges $e_p = 1.8$, $e_p = 1.5$, and $e_p = 1.3$ for JUN45, jj4b and jj4pna, respectively. The effective proton charge for each interaction was chosen to describe the ^{84}Se experimental $B(E2)$ data best. The need for adjusted effective proton charges compared to standard $e_p = 1.5$ is indicative of model space truncations, e.g., the missing neutron part of excitations in

TABLE III. Summary of the experimental and theoretical results for ^{84}Se. Experimental γ-ray transition energies are taken from NNDC. The experimental results are compared to large-scale shell-model calculations using the Ni78-II, JUN45, jj4b, and jj4pna effective interactions. In the cases of JUN45, jj4b, and jj4pna effective proton charges are chosen to overall describe experimental $B(E2)$ values best. More details are given in the text.

A	$J^{\pi i} \rightarrow J^{\pi f}$	E_γ (keV)	Experiment			Theory			
			This work / *Previous work*			$B(E2)$ (e^{2}fm^4)			
			$\frac{\sum I_D}{(\sum I_D + \sum I_T)}$	$\tau(J^\pi I)$ (ps)	$B(E2)$ (e^{2}fm^4)	Ni78-II e_p=1.7	JUN45 e_p=1.8	jj4b e_p=1.5	jj4pna e_p=1.3
^{84}Se	$2^+_1 \rightarrow 0^+_1$	1454.66(10)		*0.60(9)[1]*	*210(30)[1]*	174	210	184	202
	$4^+_1 \rightarrow 2^+_1$	666.99(7)		$29.2(^{+59}_{-37})$	$219(^{+34}_{-38})$	8	62	0.1	90
	$6^+_1 \rightarrow 4^+_1$	1248.88(13)		$12.5(^{+44}_{-28-34})$	$22(^{+22}_{-6})$				
			0.49(5)	$11.8(^{+25}_{-18-34})$	$23(^{+18}_{-4})$	45	32	71	118

TABLE IV. Experimental and theoretical excitation energies for ^{84}Se, given in keV. Experimental values are taken from NNDC.

		Experiment	Ni78-II	JUN45	jj4b	jj4pna
^{84}Se	2_1^+	1454.66(10)	1610	1550	1480	1180
	4_1^+	2121.65(10)	2010	1800	2160	3120
	6_1^+	3370.54(16)	3480	3410	3700	5190

this model space and well known for the $N = 50$ isotonic chain [1].

Furthermore, we performed calculations using the Ni78-II interaction [10,31], described above for ^{86}Se, which is also optimized for the $N = 50$ nuclei in this mass region.

Most of the calculations replicate the low-lying level scheme satisfactorily within 200 keV. The only exception is jj4pna; see Table IV.

Resulting transition probabilities can be found in Table III. Calculated values from Ni-78II, JUN45, jj4b, and jj4pna give a good description of $B(E2; 2_1^+ \rightarrow 0^+)$.

Obvious problems occur in the theoretical description of $B(E2; 4_1^+ \rightarrow 2_1^+)$; see Table III. The authors of Ref. [1] also discussed an unexpectedly high experimental cross section of the 4_1^+ state in ^{84}Se in the framework of their Coulomb excitation experiment. The calculations with NI78-II and jj4b underestimate the experimental results by factors of $\approx$27 and 2200, respectively. JUN45 and jj4pna underestimate the experimental result only by factors of $\approx$3.5 and 2.5, respectively.

These appreciable differences are investigated in more detail. The leading configurations forming low and medium spin yrast states in ^{84}Se for JUN45, jj4b, and jj4pna are given in Table V. As we regard a closed $N = 50$ neutron configuration, all calculated states come out as pure proton configurations. The highest calculated $B(E2; 4_1^+ \rightarrow 2_1^+)$ strength is given by jj4pna. This can be traced back to the distinct wave function structure of the jj4pna 4_1^+ and 2_1^+ states. From the theoretical 4_1^+ states only in jj4pna the dominant configuration is $f_{5/2}^4 p_{3/2}^2$ with 45.9% and has a large overlap with the configuration of the corresponding 2_1^+ state. In addition the jj4pna 2_1^+ wave function contains 16.1% of a $f_{5/2}^4 p_{3/2}^1 p_{1/2}^1$ configuration and lacks the $f_{5/2}^5 p_{3/2}^1$ configuration. As the jj4pna 4_1^+ includes 16.7% of a $f_{5/2}^5 p_{3/2}^1$ configuration this corresponds to an $f_{5/2} \rightarrow p_{1/2}$ stretched $E2$ transition ($\Delta l = \Delta j = 2$) which enhances the $B(E2; 4_1^+ \rightarrow 2_1^+)$ strength in the case of jj4pna. The same is true for other configurations containing one or two protons in $p_{1/2}$ orbital. The importance of $p_{1/2}$ orbital contributions for the calculated transition strengths was studied for JUN45, jj4b, and jj4pna by truncating the proton model space to $f_{5/2} p_{3/2} g_{9/2}$. When excluding the $\pi p_{1/2}$ orbital the $B(E2)$ values decreased noticeably for the lowest yrast transitions. In all cases with significant $B(E2; 2_1^+ \rightarrow 0_1^+)$ and $B(E2; 4_1^+ \rightarrow 2_1^+)$ strengths (see Table III) these were reduced by a factor of about 2 to 3 in the truncated calculations.

Additional $E2$ strength could be provided by other stretched $E2$ transitions which are not included in the current model space. One of them arises from neglecting the $\pi f_{7/2}$ orbital which is the stretched $E2$ partner of $p_{3/2}$ orbital. Further on, neutron particle-hole excitations from $g_{9/2}$ to $d_{5/2}$ would also enhance the $E2$ strengths, but are not regarded in the current valence space. We recall here that 5_1^+, 6_2^+, and 7_1^+ states in ^{84}Se represent such particle-hole neutron-core excitation, which are found directly above the yrast 6_1^+ state and significantly lower in energy than corresponding levels in heavier neighboring $N = 50$ nuclei. This points out that neutron-core excitations should be taken into account for ^{84}Se.

We notice an enhanced electric quadrupole strength for the $4_2^+ \rightarrow 2_1^+$ transition for jj4b, jj4pna, and JUN45 with $B(E2; 4_2^+ \rightarrow 2_1^+) = 222$ e^{2}fm^4, 124 e^{2}fm^4, and 57 e^{2}fm^4, respectively, and only in the case of JUN45, also the $4_3^+ \rightarrow 2_1^+$ transition has a considerable strength of 74 e^{2}fm^4. By examining the sum of the shell-model calculated $B(E2)$ strength of the lowest $4_1^+ \rightarrow 2_1^+$ transitions, one can see that $\sum_{i=1}^{3} B(E2; 4_i^+ \rightarrow 2_1^+)$ for all three interactions describes

TABLE V. Leading configurations of valence protons of low and medium spin yrast states in ^{84}Se from shell-model calculations with JUN45, jj4b, and jj4pna interactions. Numbers are given in percent. Configurations with contributions >5% for at least one interaction are given. Further details are given in the text.

Valence π	0_{gs}^+			2_1^+			4_1^+			6_1^+			4_2^+		
conf.	JUN45	jj4b	jj4pna	JUN45	jj4b	jj4pna	JUN45	jj4b	jj4pna	JUN45	jj4b	jj4pna	JUN45	jj4b	jj4pna
$f_{5/2}^6$	33.1	24.6	2.9												
$f_{5/2}^5 p_{3/2}^1$	–	–	–	28.4	2.4	–	56.8	53	16.7	–	–	–	4.9	7.9	31.5
$f_{5/2}^4 p_{3/2}^2$	40.8	43.1	70.5	41.0	51.0	62.1	13.4	8.8	45.9	79.2	67.8	79.1	69.0	64.5	29.1
$f_{5/2}^3 p_{3/2}^3$	1.0	-	2.7	3.4	9.5	7.3	14.9	19.6	23.1	14.1	22.4	13.3	7.9	4.1	7.7
$f_{5/2}^2 p_{3/2}^4$	4.4	8.6	3.3	1.3	4.0	–	1.6	1.6	–	–	–	–	–	–	–
$f_{5/2}^4 p_{3/2}^1 p_{1/2}^1$	1.1	–	5.2	5.9	7.0	16.1	1.3	1.9	2.3	–	–	–	3.2	4.5	12.4
$f_{5/2}^3 p_{3/2}^2 p_{1/2}^1$	–	–	–	4.7	5.5	4.2	2.4	2.9	3.1	–	–	1.3	3.3	7.9	11.8
$f_{5/2}^4 g_{9/2}^2$	7.31	6.4	2.9	2.6	2.0	–	1.3	1.3	1.1	–	–	–	3.2	1.5	–
$f_{5/2}^3 p_{3/2}^1 g_{9/2}^2$	–	–	–	2.2	2.8	1.3	4.2	5.5	2.8	2.2	3.6	2.3	1.6	2.3	2.6
$f_{5/2}^2 p_{3/2}^2 g_{9/2}^2$	4.0	6.5	4.0	2.2	3.6	2.0	–	1.1	–	1.7	2.4	1.5	1.6	1.7	–

the experimental value of $4_1^+ \rightarrow 2_1^+$ in the 1σ range. Only in the case of jj4b there exists one shell-model transition, i.e., $4_2^+ \rightarrow 2_1^+$, which exhausts the experimental $B(E2)$ strength for the yrast $4_1^+ \rightarrow 2_1^+$ transition. The dominating configuration of this jj4b 4_2^+ state is $f_{5/2}^4 p_{3/2}^2$ as for the 2_1^+ state. Thus, the jj4b 4_2^+ state may correspond to the experimental 4_1^+ state although the 4_2^+ state is found about 600 keV higher in energy than the experimental and shell-model 4_1^+ states.

For jj4pna the wave function of the 4_2^+ state differs from those of 4_1^+ the state. Again, we see a sizable amount of $f_{5/2}^3 p_{3/2}^2 p_{1/2}^1$ configuration including the $p_{1/2}$ orbital allowing for a stretched $E2$ transition towards a $f_{5/2}^4 p_{3/2}^2$ configuration in 2_1^+. The above discussion on the $4_1^+ \rightarrow 2_1^+$ transition strength suggests a possible need to modify the used interactions.

The comparison between the experimental and theoretical $B(E2; 6_1^+ \rightarrow 4_1^+)$ values shows that Ni78-II and JUN45 describe the experimental result reasonably well (see Table III). In case of jj4b and jj4pna the calculated transition strengths overestimate the experimental result, but values are of the same magnitude. It is worth mentioning that by excluding the $p_{1/2}$ orbital, the $B(E2; 6_1^+ \rightarrow 4_1^+)$ strength is not much affected for jj4b and jj4pna and stays constant in the case of JUN45. Therefore we conclude that the role of the $p_{1/2}$ shell is subordinate for this transition.

The overall best agreement with the experimental $B(E2)$ values is given by JUN45. This fact together with the excellent reproduction of experimental excitation energies supports the spin and parity assignment of the $E = 3370$ keV level as the yrast 6_1^+ state.

V. CONCLUSION

In summary, lowest yrast states in ^{84,86}Se were populated and their level lifetimes were measured with the recoil distance Doppler shift technique.

In the case of ^{86}Se the $B(E2; 2_1^+ \rightarrow 0_1^+)$ from the level lifetime of the 2_1^+ state and a lower $B(E2)$ limit from the effective level lifetime of the 4_1^+ state were determined. This enabled a first testing of shell-model predictions concerning $B(E2)$ values beyond the $N = 50$ shell closure. In ^{86}Se, in addition to the good reproduction of the yrast energy spectra, shell-model calculations perform fairly well in reproducing the $2_1^+ \rightarrow 0_1^+$ transition strength. Analyzing the intrinsic nuclear shape parameters, we suggest a more triaxial shape for ^{86}Se compared to ^{88}Se. For further discussions the experimental $B(E2)$ values for the $4_1^+ \rightarrow 2_1^+$ transition and, even more interesting, for the $6_1^+ \rightarrow 4_1^+$ are of high importance.

In case of ^{84}Se $4_1^+ \rightarrow 2_1^+$ and $6_1^+ \rightarrow 4_1^+$ $E2$ transition strengths were determined from the level lifetimes of the 4_1^+ and 6_1^+ states. Shell-model calculations of ^{84}Se using different effective interactions perform fairly well for the $2_1^+ \rightarrow 0_1^+$ transition. Further on, all calculations experience problems in reproducing the yrast $4_1^+ \rightarrow 2_1^+$ transition strength. Calculated $B(E2; 4_1^+ \rightarrow 2_1^+)$ values differ from experimental ones with up to three orders of magnitude. These results are discussed in terms of valence protons leading configurations for the low- and medium-spin yrast states. In addition, truncated calculations support the importance of $p_{1/2}$ orbital contributions which allow for strong $p_{1/2} \leftrightarrow f_{5/2}$ stretched $E2$ transitions.

The $6_1^+ \rightarrow 4_1^+$ transition can be described best with JUN45, but also calculations with Ni78-II and jj4b perform well. The overall good agreement of both, calculated excitation energy and $B(E2)$ value of the yrast 6_1^+ state in ^{84}Se supports the spin and parity assignment of the $E = 3370$ keV level as the yrast 6_1^+ state.

Future calculations with larger valence spaces allowing the $\nu g_{9/2} \leftrightarrow d_{5/2}$ orbital to account for neutron particle-hole excitations or the $\pi f_{7/2} \leftrightarrow p_{3/2}$ stretched $E2$ transitions would be of interest in the $N = 50$ isotones.

ACKNOWLEDGMENTS

This work was partially supported by the European Union Seventh Framework Program FP7/2007-2013 under Grant Agreement No. 262010 ENSAR and by the German Research Foundation (DPG) under Contract No. DE 1516/3-1. J.L. thanks the Bonn-Cologne Graduate School of Physics and Astronomy (BCGS) for financial support.

[1] A. Gade, T. Baugher, D. Bazin, B. A. Brown, C. M. Campbell, T. Glasmacher, G. F. Grinyer, M. Honma, S. McDaniel, R. Meharchand, T. Otsuka, A. Ratkiewicz, J. A. Tostevin, K. A. Walsh, and D. Weisshaar, Phys. Rev. C **81**, 064326 (2010).
[2] Y. H. Zhang *et al.*, Phys. Rev. C **70**, 024301 (2004).
[3] P. C. Srivastava and M. J. Ermamatov, Phys. Scr. **88**, 045201 (2013).
[4] A. Prévost *et al.*, Eur. Phys. J. A **22**, 391 (2004).
[5] F. Drouet *et al.*, EPJ Web of Conferences **62**, 01005 (2013).
[6] G. A. Jones *et al.*, Phys. Rev. C **76**, 054317 (2007).
[7] E. F. Jones *et al.*, Phys. Rev. C **73**, 017301 (2006).
[8] K. Sieja, T. R. Rodríguez, K. Kolos, and D. Verney, Phys. Rev. C **88**, 034327 (2013).
[9] M. Czerwiński, T. Rząca-Urban, K. Sieja, H. Sliwinska, W. Urban, A. G. Smith, J. F. Smith, G. S. Simpson, I. Ahmad, J. P. Greene, and T. Materna, Phys. Rev. C **88**, 044314 (2013).
[10] T. Materna, W. Urban, K. Sieja, U. Köster, H. Faust, M. Czerwiński, T. Rząca-Urban, C. Bernards, C. Fransen, J. Jolie, J.-M. Regis, T. Thomas, and N. Warr, Phys. Rev. C **92**, 034305 (2015).
[11] G. Winter, R. Schwengner, J. Reif, H. Prade, L. Funke, R. Wirowski, N. Nicolay, A. Dewald, P. von Brentano, H. Grawe, and R. Schubart, Phys. Rev. C **48**, 1010 (1993).
[12] A. Dewald, O. Möller, and P. Petkov, Prog. Part. Nucl. Phys. **67**, 786 (2012).
[13] D. Montanari, Ph.D thesis, University of Milan, Italy, 2009.
[14] A. Stefanini *et al.*, Nucl. Phys. A **701**, 217 (2002).
[15] S. Szilner *et al.*, Phys. Rev. C **76**, 024604 (2007).
[16] L. Corradi *et al.*, Nucl. Instrum. Methods Phys. Res. B **317**, 743 (2013).
[17] A. Gadea *et al.*, Nucl. Instrum. Methods Phys. Res. A **654**, 88 (2011).
[18] S. Akkoyun *et al.*, Nucl. Instrum. Methods Phys. Res. A **668**, 26 (2012).
[19] A. Wiens, H. Hess, B. Birkenbach, B. Bruyneel, J. Eberth, D. Lersch, G. Pascovici, P. Reiter, and H.-G.

Thomas, Nucl. Instrum. Methods Phys. Res. A **618**, 223 (2010).
[20] A. Winther, Nucl. Phys. A **572**, 191 (1994).
[21] A. B. Brown, C. W. Snyder, W. A. Fowler, and C. C. Lauritsen, Phys. Rev. **82**, 159 (1951).
[22] T. K. Alexander and A. Bell, Nucl. Instrum. Methods **81**, 22 (1970).
[23] K.-H. Speidel, N. Benczer-Koller, G. Kumbartzki, C. Barton, A. Gelberg, J. Holden, G. Jakob, N. Matt, R. H. Mayer, M. Satteson, R. Tanczyn, and L. Weissman, Phys. Rev. C **57**, 2181 (1998).
[24] O. Tarasov and D. Bazin, Nucl. Instrum. Methods Phys. Res. B **204**, 174 (2003).
[25] S. Agostinelli *et al.*, Nucl. Instrum. Methods Phys. Res. Section A: Accelerators, Spectrometers, Detectors and Associated Equipment **506**, 250 (2003).
[26] B. Birkenbach, Ph.D thesis, University of Cologne, 2014.
[27] P. Hoff *et al.*, Z. Phys. A **338**, 285 (1991).
[28] E. Caurier and F. Nowacki, Acta Phys. Pol. B **30**, 705 (1999).
[29] E. Caurier, G. Martínez-Pinedo, F. Nowacki, A. Poves, and A. P. Zuker, Rev. Mod. Phys. **77**, 427 (2005).
[30] K. Sieja, F. Nowacki, K. Langanke, and G. Martínez-Pinedo, Phys. Rev. C **79**, 064310 (2009).
[31] M. Czerwiński *et al.*, Phys. Rev. C **92**, 014328 (2015).
[32] K. Kumar, Phys. Rev. Lett. **28**, 249 (1972).
[33] M. Honma, T. Otsuka, T. Mizusaki, and M. Hjorth-Jensen, Phys. Rev. C **80**, 064323 (2009).
[34] D. Verney *et al.* (PARRNe Collaboration), Phys. Rev. C **76**, 054312 (2007).
[35] B. Brown and W. Rae, Nucl. Data Sheets **120**, 115 (2014).